PNAS RESEARCH ARTICLE | IMMUNOLOGY AND INFLAMMATION

PBLD enhances antiviral innate immunity by promoting the p53–USP4–MAVS signaling axis

Fengyun Chu[a,1], Peili Hou[a,b,1], Hongchao Zhu[a], Yan Gao[a], Xiaomeng Wang[a], Wenqi He[c], Juan Ren[a], Min Li[a], Yu Liu[a], Daniel Chang He[d], Hongmei Wang[a,2], Yuwei Gao[e,2], and Hongbin He[a,b,2]

Affiliations are included on p. 12.

Edited by Katherine Fitzgerald, University of Massachusetts Medical School, Worcester, MA; received January 18, 2024; accepted August 22, 2024

Phenazine biosynthesis-like domain-containing protein (PBLD) has been reported to be involved in the development of many cancers. However, whether PBLD regulates innate immune responses and viral replication is unclear. In this study, although it was found that the activity of PBLD extends to other PRRs, we focused on the RLR pathway activated via the p53–USP4–MAVS axis in response to virus infections. We found that PBLD deubiquitinates and stabilizes MAVS through ubiquitin-specific protease 4 (USP4) to promote antiviral innate immunity. Mechanistically, PBLD activates the transcription of USP4 via the upregulation of p53. USP4, which is a MAVS-interacting protein, substantially stabilizes the MAVS protein by deconjugating K48-linked ubiquitination chains from the MAVS protein at Lys461 during RNA virus infection. Most intriguingly, RNA virus-infected primary macrophages (peritoneal macrophages, PMs, and bone marrow–derived macrophages, BMDMs) and internal organ cells (lung and liver) from PBLD-deficient mice suppress the IFN-I response and promote viral replication. Notably, PBLD-deficient mice are more susceptible to RNA virus infection than their wild-type littermates. Our findings highlight a unique function of PBLD in antiviral innate immunity through the p53–USP4–MAVS signaling, providing a preliminary basis for research on PBLD as a target molecule for treating RNA virus infection.

PBLD | MAVS | USP4 | RNA viruses | Type I IFN

Significance

Combating viral infections has become a paramount global concern. The innate immune response serves as the first line of defense against invading pathogens. Currently, phenazine biosynthesis-like domain-containing protein (PBLD) as a tumor suppressor has been reported to be involved in the development of many cancers. However, whether PBLD regulates innate immune responses and viral replication is unclear. Here, we found that PBLD enhances the antiviral innate immune response against RNA viruses, thereby inhibiting their replication both in vitro and in vivo by promoting the p53–USP4–MAVS signaling axis. Consequently, the PBLD-mediated regulation of the antiviral immune response plays a critical role in determining virus replication for developing drugs to combat RNA virus-mediated pandemics.

Highly infectious and pathogenic viruses can lead to severe clinical symptoms and even fatalities (1, 2). For instance, influenza A viruses (IAVs), which are significant zoonotic pathogens, are widely distributed in nature and remain a substantial threat to animal and human health. Understanding the interactions between viruses and their hosts is crucial for the development of effective therapeutic drugs.

The innate immune system serves as the primary defense mechanism against invading pathogens and is activated by pathogen-associated molecular patterns (PAMPs), which are recognized by pattern recognition receptors (PRRs) that are encoded in the germline (3, 4). Retinoic acid-inducible gene I protein (RIG-I)-like receptors, particularly RIG-I, primarily detect cytosolic RNA. Upon the detection of RNA viruses, RIG-I undergoes conformational changes and interacts with the caspase activation and recruitment domain (CARD) of the mitochondrial antiviral signaling (MAVS) protein through its N-terminal tandem CARD, resulting in the formation of prion-like MAVS aggregates (5–8). Subsequent activation of TBK1/IKKε and phosphorylation of the transcription factors IRF3/IRF7 and NF-κB induce the expression of type-I interferons (IFNs), interferon-stimulated genes (ISGs), and proinflammatory cytokines, thereby eliciting antiviral immune responses.

MAVS, which serves as an adaptor protein, plays a pivotal role in connecting virus recognition to downstream antiviral kinase cascades (9, 10). Nevertheless, the activity and stability of MAVS are intricately regulated by various posttranscriptional mechanisms, such as phosphorylation, ubiquitination, and deubiquitylation, which are crucial for its proper function (11–13). E3-mediated ubiquitination strongly influences the stability and availability of MAVS. The identification of deubiquitinating enzymes (DUBs) that remove poly or monoubiquitin chains from their targets to counterbalance E3-mediated ubiquitination has been an emerging field of study. Regarding the deubiquitination of MAVS, recent research has highlighted the involvement of OTUD4 and OTUD1 (14, 15). However, whether other DUBs contribute to the regulation of MAVS ubiquitination, thereby maintaining its expression stability in a precise and spatial manner, requires further investigation.

Phenazine biosynthesis-like domain-containing protein (PBLD), also known as MAWBP, is highly expressed in several visceral organs, including the heart, lungs, and liver. PBLD acts as a tumor suppressor, regulating the occurrence and development of various cancers (16, 17). Recent research has indicated that PBLD hinders microenvironmental cross talk

Author contributions: P.H., H.W., Y.G., and H.H. designed research; F.C., H.Z., Y.G., X.W., J.R., M.L., Y.L., and D.C.H. performed research; F.C., P.H., H.Z., X.W., W.H., J.R., M.L., Y.L., D.C.H., H.W., Y.G., and H.H. analyzed data; and F.C., P.H., D.C.H., and H.H. wrote the paper.

The authors declare no competing interest.

This article is a PNAS Direct Submission.

[1]F.C. and P.H. contributed equally to this work.

[2]To whom correspondence may be addressed. Email: hongmeiwang@sdnu.edu.cn, yuwei0901@outlook.com, or hongbinhe@sdnu.edu.cn.

This article contains supporting information online at https://www.pnas.org/lookup/suppl/doi:10.1073/pnas.2401174121/-/DCSupplemental.

Published November 26, 2024.

between hepatocellular carcinoma (HCC) cells and endothelial cells, thereby playing a crucial role in angiogenesis (18). Likewise, PBLD impedes the growth and invasion of HCC cells by affecting multiple genes associated with the NF-κB, MAPK, and epithelial–mesenchymal transition (EMT) signaling pathways (19). Additionally, PBLD is involved in regulating inflammatory diseases. For instance, PBLD inhibits NF-κB signaling, leading to reduced inflammatory mediator production and decreased colonic inflammation (20). However, the roles of PBLD in the IFN-I signaling pathway, viral infection, and virus replication have not been explored.

In this study, we investigated the potential impact of PBLD on the signaling pathways affected by type I IFNs triggered by RNA viruses, including bovine epidemic fever virus (BEFV), vesicular stomatitis virus (VSV), and IAVs (H1N1). Our data suggest that PBLD functions as a positive regulator of RLR signaling pathways by stabilizing MAVS, consequently inhibiting RNA replication both in vitro and in vivo. Furthermore, we found that PBLD activates the transcription of USP4 via p53 during RNA virus infection. As a DUB, USP4 binds to MAVS via its DUSP domain and subsequently inhibits its K48-linked ubiquitination-mediated degradation to maintain the stability of the MAVS protein. Overall, our findings unveil a unique role of PBLD in the antiviral IFN-I response. Specifically, PBLD promotes the p53–USP4–MAVS signaling axis, leading to an increase in the IFN-I response against RNA virus infection. This finding provides valuable insight into the development of targeted antiviral agents.

Results

PBLD Inhibits the Replication of BEFV, VSV, and H1N1 Viruses. This study initially identified *PBLD* as a gene that is strongly downregulated during viral infection via transcriptomic analysis of virus-infected and uninfected cells (*SI Appendix*, Fig. S1*A*). We found multiple viral infections at indicated time points reduced PBLD expression at the transcriptional and protein levels (*SI Appendix*, Fig. S8 *A–F*), which suggested that the downregulation of PBLD expression during virus infection may function via (common) viral effectors. To investigate the function of PBLD during virus infection, recombinant plasmids containing the PBLD gene from golden hamsters and humans were constructed, and MDBK cell lines stably expressing Flag epitope-tagged PBLD and negative control cell lines (Ctrl) were successfully generated. Remarkably, overexpression of PBLD was found to inhibit the replication of BEFV. This was evident from the reduced expression levels of the BEFV *N* gene at both the mRNA (*SI Appendix*, Fig. S1*B*) and protein (Fig. 1*A* and *SI Appendix*, Fig. S1*C*) levels, as well as the decreased viral titer of the 50% tissue culture infective dosage ($TCID_{50}$) per milliliter of BEFV (Fig. 1*B* and *SI Appendix*, Fig. S1*D*) in virus-infected BHK-21 cells and MDBK cells compared with those in the control groups. Similarly, the VSV *N* and H1N1 *NP* gene mRNA levels (*SI Appendix*, Fig. S1*E*), the G and NP protein levels (Fig. 1 *C* and *D*), the VSV and H1N1 titers (Fig. 1 *E* and *F*), and the VSV GFP intensity (Fig. 1*G* and *SI Appendix*, Fig. S1*F*) were decreased in VSV infected PBLD-overexpressing HeLa cells and H1N1 infected A549 cells.

Then, the effects of silencing or knocking out PBLD on viral replication were determined. We first verified the expression of PBLD (*SI Appendix*, Fig. S1*G*). We noted that BEFV infection resulted in a decrease in PBLD-knockout (KO) MDBK cell lines that were generated via the CRISPR/Cas9 technique, as indicated by increased mRNA and protein expression of the BEFV N gene (Fig. 1*H* and *SI Appendix*, Fig. S1*H*) and an increased BEFV titer by nearly 8-fold (Fig. 1*I*). In addition, compared with transfection with control siRNA, transfection with a PBLD-specific small interfering RNA (siRNA) in BHK-21 cells resulted in enhanced replication of BEFV (*SI Appendix*, Fig. S1 *H–J*), Similarly, knockdown of PBLD in HeLa cells or A549 cells increased the viral gene and protein expression of VSV or H1N1 (Fig. 1 *J* and *K* and *SI Appendix*, Fig. S1*K*), respectively, as well as the VSV and H1N1 titers (Fig. 1 *L* and *M*) and VSV-GFP intensity (Fig. 1*N* and *SI Appendix*, Fig. S1*L*).

To further confirm the effect of PBLD on antiviral immune responses, we utilized CRISPR/Cas9-mediated genome editing to generate PBLD-deficient ($Pbld^{-/-}$) mice (*SI Appendix*, Fig. S1*M*). PCR-based genotyping analysis of genomic DNA from tail samples confirmed the $Pbld^{+/-}$ mouse offspring and allowed the differentiation of $Pbld^{+/+}$, $Pbld^{+/-}$, and $Pbld^{-/-}$ mice (*SI Appendix*, Fig. S1*N*). Moreover, the $Pbld^{-/-}$ mice exhibited normal growth and development, similar to their wild-type littermates. The western blotting results showed that the deficiency of PBLD in the lung and liver tissues of $Pbld^{-/-}$ mice was clearly evident (*SI Appendix*, Fig. S1*O*). We then measured the expression of the VSV *N* gene or BEFV *N* gene and the virus titer in murine primary macrophages obtained from $Pbld^{+/+}$ or $Pbld^{-/-}$ mice. As expected, PBLD knockout markedly increased the replication of VSV and BEFV in PMs and BMDMs, respectively (*SI Appendix*, Fig. S1 *P* and *Q*). Taken together, our results indicate that PBLD inhibits the replication of the BEFV, VSV, and H1N1 viruses.

PBLD Augments Type-I IFN Signaling During RNA Virus Infection. The IFN-I signaling pathway plays a critical role in the antiviral immune response (21, 22). We found that overexpression PBLD increased mRNA expression of *Ifnα4, Ifnb, Isg15,* and *Mx1* via RLRs, TLRs, and cGAS/STING respective stimuli (*SI Appendix*, Fig. S9*A*). Consistently, the opposite results were observed in PBLD-knockout cells (*SI Appendix*, Fig. S9*B*). However, we also found that there was no difference on the expression of IFN/ISGs induced by VSV infection in the STING-knockout cells or added the inhibitor of TLR3 (CU-CPT 4a) and TLR4 (TLR-IN-C34) (*SI Appendix*, Fig. S9*C*). A luciferase reporter assay revealed that compared with control treatment, PBLD overexpression significantly increased the activation of the IFN-β promoter in HEK293T cells upon VSV stimulation (Fig. 2*A*). Moreover, overexpression of PBLD up-regulated the mRNA levels of *Ifnb* (Fig. 2*B*) and downstream ISGs (*SI Appendix*, Fig. S2 *A* and *B*) in both MDBK cells and BHK-21 cells during BEFV infection compared with those in the control groups. Furthermore, these results were validated in PBLD-overexpressing HeLa cells infected with VSV or treated with poly(I:C) (Fig. 2*C* and *SI Appendix*, Fig. S2*C*) as well as A549 cells infected with H1N1 (Fig. 2*D* and *SI Appendix*, Fig. S2*D*).

Conversely, compared with control treatment, PBLD silencing significantly decreased the activation of the IFN-β promoter in HEK293T cells upon VSV stimulation (Fig. 2*E*). Knockout or knockdown of PBLD in MDBK cells or BHK-21 cells resulted in the inhibition of BEFV-induced mRNA expression of *Ifnb*, *Isg15,* and *Mx1* at different time points (Fig. 2*F* and *SI Appendix*, Fig. S2 *E* and *F*). Similarly, the knockdown of PBLD in HeLa cells and A549 cells also significantly suppressed the increase in the mRNA expression of *Ifnb*, *Isg15*, and *Mx1* induced by VSV, poly(I:C), or H1N1 (Fig. 2 *G* and *H* and *SI Appendix*, Fig. S2 *G* and *H*). We further verified these findings in PMs (Fig. 2*I* and *SI Appendix*, Fig. S2*I*) and BMDMs (Fig. 2*J* and *SI Appendix*, Fig. S2*J*) from $Pbld^{+/+}$ and $Pbld^{-/-}$ mice. Importantly, when PMs and BMDMs were treated with poly(I:C), the results also revealed lower mRNA expression of *Ifnα4, Ifnb, Isg15,* and *Isg56* with *Pbld* deficiency (Fig. 2 *K* and *L*). Consistent with these findings, PBLD deficiency led to a notable reduction in the protein expression of IFN-α and IFN-β in PMs after VSV and BEFV infection (Fig. 2 *M* and *N*)

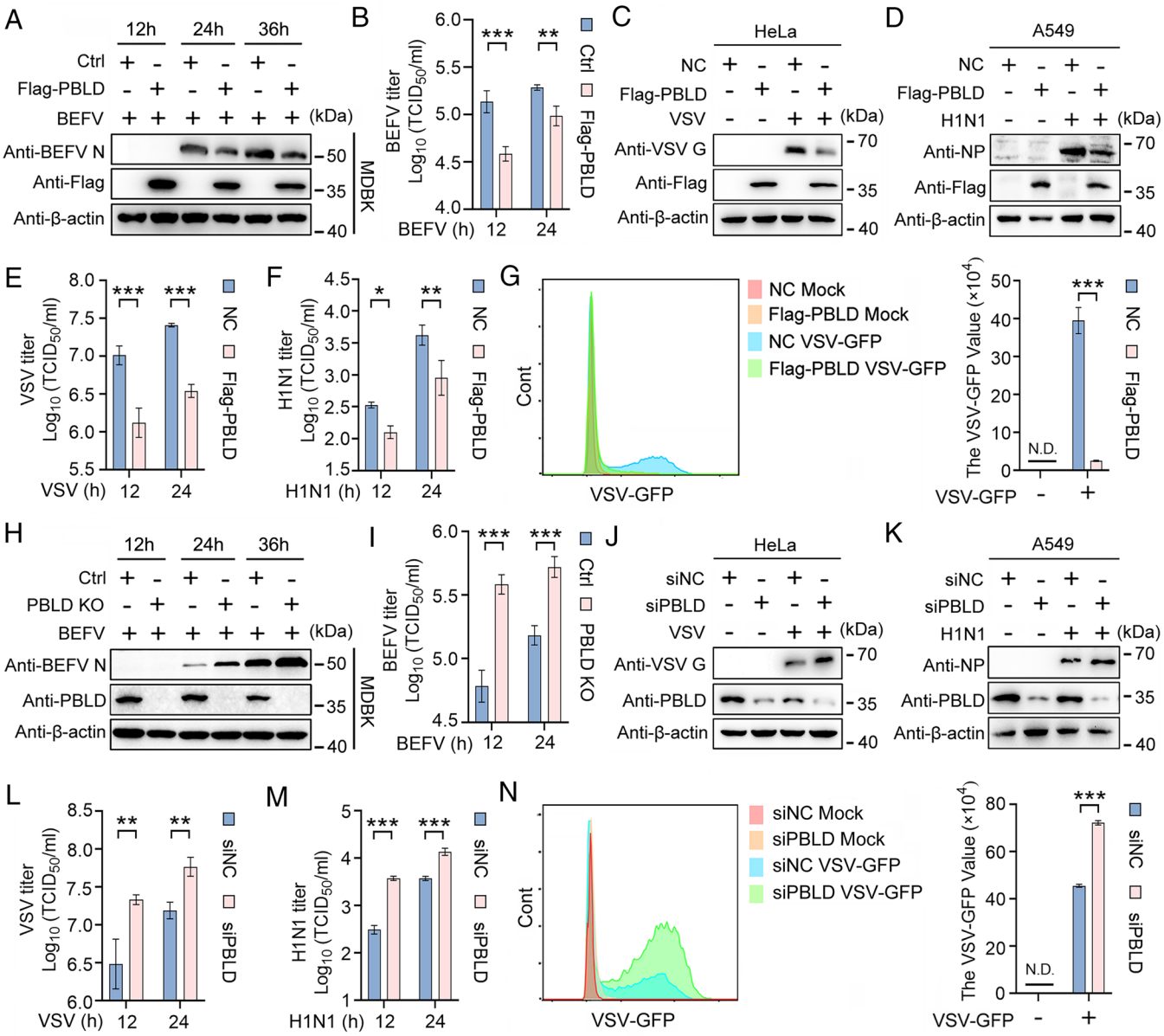

Fig. 1. PBLD inhibits BEFV, VSV, and H1N1 replication. (*A* and *B*) Western blotting analysis of the expression levels of the protein of the viruses (*A*) and $TCID_{50}$ assays of the viral titers (*B*) in PBLD-overexpressing MDBK cell lines infected with BEFV [multiplicity of infection (MOI) = 0.1] for the indicated durations. (*C*–*F*) Western blotting analysis of the expression levels of the proteins of VSV (*C*) and H1N1(*D*), and $TCID_{50}$ assays of the viral titers in PBLD-overexpressing HeLa cells (*E*) and A549 cells (*F*) infected with VSV (MOI = 0.1) or H1N1 (MOI = 1) virus at the indicated time points. (*G*) GFP intensity in PBLD-overexpression and control cells infected with VSV-GFP (MOI = 0.1) for 12 h was determined by flow cytometry. The quantitative analysis of GFP intensity of VSV (*Right*). (*H* and *I*) Western blotting analysis of the expression levels of the protein of the viruses (*H*) and $TCID_{50}$ analysis of the viral titers (*I*) in the PBLD KO MDBK cell lines infected with BEFV (MOI = 0.1) for the indicated durations. (*J*–*M*) Western blotting analysis of the expression levels of the protein of VSV (*J*) and H1N1 (*K*) and $TCID_{50}$ analysis of the viral titers in PBLD-silenced HeLa cells (*L*) and A549 cells (*M*) infected with VSV (MOI = 0.1) or H1N1 (MOI = 1) virus for the indicated durations. (*N*) GFP intensity in PBLD-silenced HeLa cells and control cells infected with VSV-GFP (MOI = 0.1) or mock infection for 12 h was determined by flow cytometry. The quantitative analysis of GFP intensity of VSV (*Right*). Data in (*A*, *C*, *D*, *H*, *J*, and *K*) are representative of one of three independent experiments. Data in (*B*, *E*, *F*, *G*, *I*, *L*, *M*, *N*) are presented as mean ± SD from three independent experiments, Student's *t* test or two-way ANOVA. $*P < 0.05$, $**P < 0.01$, and $***P < 0.001$.

or in PMs and BMDMs treated with poly(I:C) (Fig. 2 *O* and *P*). Overall, these findings demonstrate that PBLD promotes the RNA virus infection-induced IFN-I signaling pathway.

PBLD Enhances Type-I IFN Signaling by Up-Regulating MAVS. To investigate the regulatory mechanisms of PBLD in type-I IFN signaling, we conducted a luciferase reporter assay to measure the activation of the IFN-β promoter and the IFN-stimulated response element (ISRE) promoter in response to the RIG-I signaling cascade both in the presence and absence of PBLD. Our results indicated that PBLD overexpression promoted the activation of luciferase reporters induced by RIG-I-N (the N-terminal CARD of RIG-I) and MAVS but not by TBK1 or IRF3-5D (a constitutively activated form of IRF3) (23), and PBLD knockdown had the opposite results (Fig. 3 *A* and *B* and *SI Appendix*, Fig. S3 *A* and *B*). Furthermore, analysis of the protein expression of RIG-I signaling cascades revealed that PBLD overexpression significantly up-regulated the MAVS, phosphorylated TBK1 (p-TBK1), and ISG15 levels in MDBK and BHK-21 cells after BEFV infection (Fig. 3*C* and *SI Appendix*, Fig. S3*C*). Similar results were observed for the overexpression of PBLD in HeLa cells infected with VSV, those transfected with poly(I:C), or A549 cells infected with H1N1 (Fig. 3*C*). Importantly, PBLD increased MAVS protein expression in a dose-dependent manner (*SI Appendix*, Fig. S3*D*).

Furthermore, the regulation of MAVS expression by PBLD was investigated in the context of PBLD knockdown or knockout.

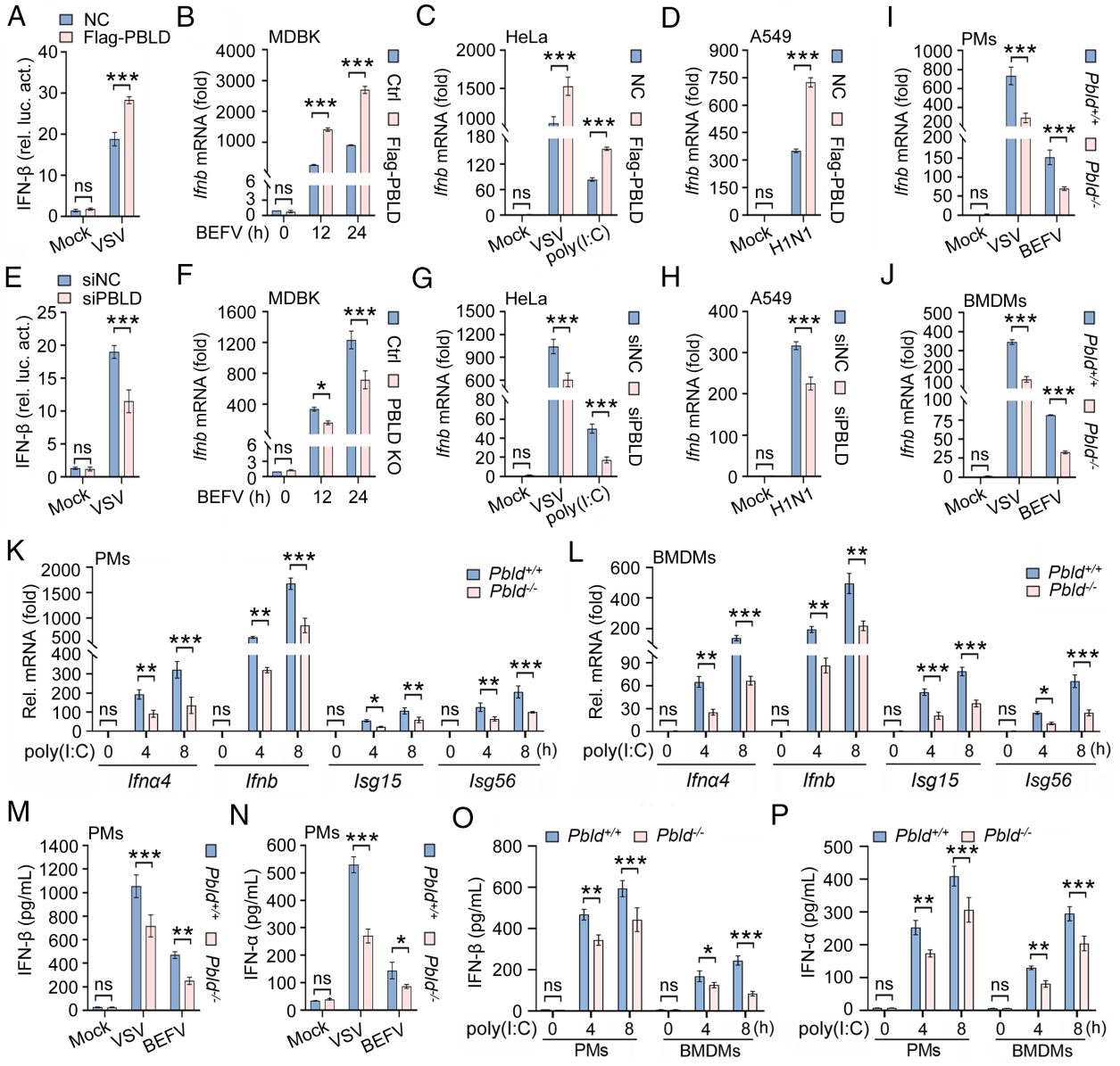

Fig. 2. PBLD promotes the RNA virus infection–induced type I IFN signaling pathway. (*A*) Luciferase reporter assays of HEK293T cells transfected with IFN-β-Luc promoter plasmids, pRL-TK (*Renilla* luciferase reporter plasmids), the indicated expression plasmids together with Flag-PBLD or empty vector and infected with VSV (MOI = 0.1) for 12 h. (*B–D*) Real-time PCR analysis of *Ifnb* mRNA expression in PBLD-overexpressing MDBK cell lines infected with BEFV (MOI = 0.1) for the indicated time points (*B*), HeLa cells with PBLD-overexpression infected with VSV (MOI = 0.1) for 12 h or transfected with low-molecular-weight (LMW) poly(I:C) (10 μg/mL) for 4 h (*C*), and A549 cells infected with H1N1 (MOI = 1) for 24 h (*D*). (*E*) Luciferase reporter assays were performed with HEK293T cells transfected with IFN-β-Luc promoter plasmids, pRL-TK, PBLD-specific siRNA (siPBLD), or negative control siRNA (siNC) and infected with VSV (MOI = 0.1) for 12 h. (*F–H*) Real-time PCR analysis of the mRNA expression of *Ifnb* in PBLD KO MDBK cells infected with BEFV (MOI = 0.1) for the indicated time points (*F*), HeLa cells upon transfection with siPBLD or siNC infected with VSV (MOI = 0.1) for 12 h or transfected with LMW poly(I:C) (10 μg/mL) for 4 h (*G*), and A549 cells infected with H1N1 (MOI = 1) for 24 h (*H*). (*I* and *J*) Real-time PCR analysis of the mRNA levels of *Ifnb* in PMs (*I*) and BMDMs (*J*) from *Pbld*$^{+/+}$ and *Pbld*$^{-/-}$ mice infected with VSV (MOI = 0.1) and BEFV (MOI = 0.1) for 12 h, respectively. (*K* and *L*) Real-time PCR analysis of *Ifnα4, Ifnb, Isg15,* and *Isg56* mRNA expression in PMs (*K*) and BMDMs (*L*) from *Pbld*$^{+/+}$ and *Pbld*$^{-/-}$ mice transfected with LMW poly(I:C) (10 μg /mL) for 4 h and 8 h. (*M* and *N*) ELISA of IFN-β and IFN-α levels in the supernatants of PMs from *Pbld*$^{+/+}$ and *Pbld*$^{-/-}$ mice infected with VSV (MOI = 0.1) and BEFV (MOI = 0.1) for 12 h, respectively. (*O* and *P*) ELISA of IFN-β and IFN-α levels in the supernatants of PMs (*O*) and BMDMs (*P*) from *Pbld*$^{+/+}$ and *Pbld*$^{-/-}$ mice transfected with LMW poly(I:C) (10 μg /mL) for 4 h and 8 h. All the data are presented as mean ± SD from three independent experiments, ns (not significant) $P > 0.05$, $^{*}P < 0.05$, $^{**}P < 0.01$, and $^{***}P < 0.001$ (two-way ANOVA in all the analyses).

The expression of MAVS, p-TBK1, and ISG15 was markedly decreased in PBLD-knockdown BHK-21 cells following BEFV infection, as was the case in the PBLD-KO MDBK cell line (Fig. 3*D* and *SI Appendix*, Fig.S3*E*). Similarly, silencing or knockout of PBLD led to a reduction in the protein levels of MAVS, p-TBK1, and ISG15 in HeLa cells infected with VSV or treated with poly(I:C), A549 cells infected with H1N1 (Fig. 3*D*), and PMs and BMDMs from *Pbld*$^{-/-}$ mice infected with VSV (Fig. 3 *E* and *F*). Subsequently, we constructed MAVS-knockout cells (*SI Appendix*, Fig. S5*I*) and found that PBLD specificity increase RLR/MAVS-signaling to combat virus infection through detecting the VSV titer in MAVS KO cells compared with the controls (*SI Appendix*, Fig. S9*D*). Moreover, an immunoprecipitation assay revealed that there was no interaction between PBLD and MAVS regardless of whether the cells were stimulated with VSV or not, indicating that PBLD indirectly up-regulates MAVS (*SI Appendix*, Fig. S3*F*). In conclusion, PBLD enhances IFN-I signaling through the upregulation of MAVS expression.

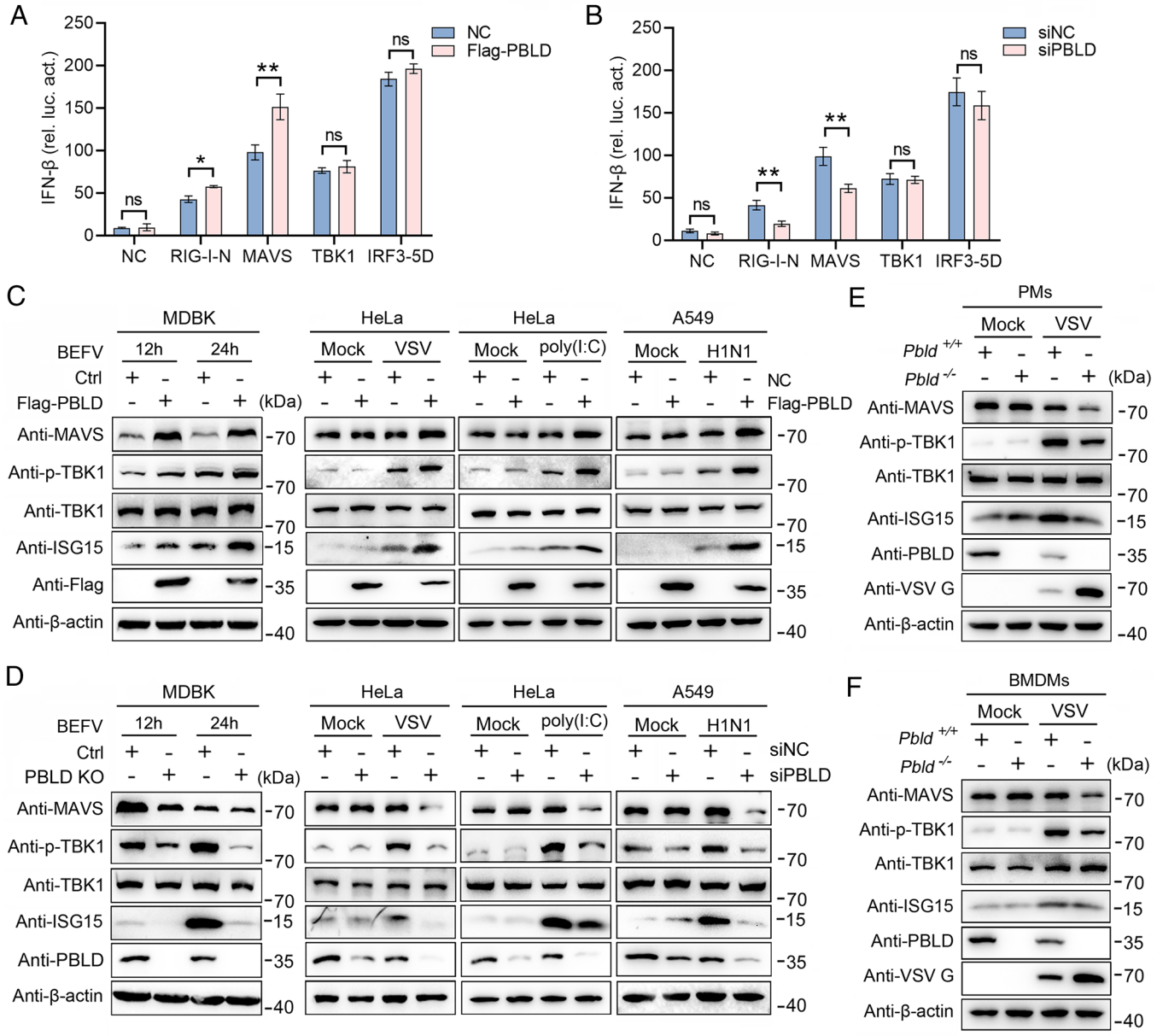

Fig. 3. PBLD positively regulates the type I IFN response by stabilizing MAVS. (*A* and *B*) Luciferase reporter assays of HEK293T cells transfected with IFN-β-Luc promoter plasmids, pRL-TK, or 300 ng of the indicated plasmids [Flag-RIG-I (N), Flag-MAVS, HA-TBK1, HA-IRF3 (5D)], together with Flag-PBLD (*A*) or siPBLD (*B*) and empty vector for 24 h. (*C*) Western blotting analysis of the protein expression of MAVS, p-TBK1, TBK1, ISG15, Flag, and β-actin in PBLD-overexpressing MDBK cell lines infected with BEFV (MOI = 0.1) for the indicated time points; HeLa cells infected with VSV (MOI = 0.1) for 12 h or transfected with LMW poly(I:C) (10 μg/mL) for 4 h; and A549 cells infected with H1N1 (MOI = 1) for 24 h. (*D*) Western blotting analysis of the protein expression of MAVS, p-TBK1, TBK1, ISG15, PBLD, and β-actin in PBLD KO MDBK cell lines infected with BEFV (MOI = 0.1) for the indicated times, and transfected with siPBLD or siNC in HeLa cells infected with VSV (MOI = 0.1) for 12 h or transfected with LMW poly(I:C) (10 μg/mL) for 4 h; and A549 cells infected with H1N1 (MOI = 1) for 24 h. (*E* and *F*) Western blotting analysis of the indicated proteins in PMs (*E*) and BMDMs (*F*) from $Pbld^{+/+}$ and $Pbld^{-/-}$ mice infected with VSV (MOI = 0.1) for 12 h, respectively. Data in (*C*–*F*) are representative of one of three independent experiments. Data in (*A* and *B*) are presented as mean ± SD from three independent experiments, Student's *t* test, ns $P > 0.05$, $^{*}P < 0.05$, $^{**}P < 0.01$.

PBLD Inhibits the K48-Linked Polyubiquitination of MAVS. To elucidate the role of PBLD in the upregulation of MAVS expression, we investigated the mRNA levels of *Mavs* in BEFV-infected BHK-21 cells, VSV-infected HeLa cells, and H1N1-infected A549 cells. Our results show that overexpression or knockdown of PBLD did not impact the mRNA level of *Mavs* induced by BEFV, VSV, or H1N1 viral infection (*SI Appendix*, Fig. S4 *A* and *B*). Moreover, the silencing of PBLD accelerated the degradation of MAVS both in the presence of cycloheximide (CHX, a protein biosynthesis inhibitor) during VSV and BEFV infection but did not affect cells that were not infected with a virus (Fig. 4*A* and *SI Appendix*, Fig. S4 *C* and *D*), indicating that PBLD modulates the expression of the MAVS protein at the posttranslational level during virus infection to enhance the antiviral immune response. Subsequently, we explored the regulatory mechanisms underlying PBLD-mediated MAVS stabilization. Our findings demonstrated that the degradation of MAVS induced by PBLD knockdown was inhibited by MG132, which is a proteasome inhibitor, but not by the autophagy inhibitor chloroquine (CQ) compared with that in the control groups of VSV-infected HeLa cells or BEFV-infected BHK-21 cells, and the MAVS protein levels did not change in PBLD knockdown cells without virus infection (Fig. 4*B* and *SI Appendix* Fig. S4 *E* and *F*). These findings suggest that PBLD plays a critical role in the stabilization of MAVS by suppressing the ubiquitin–proteasome system.

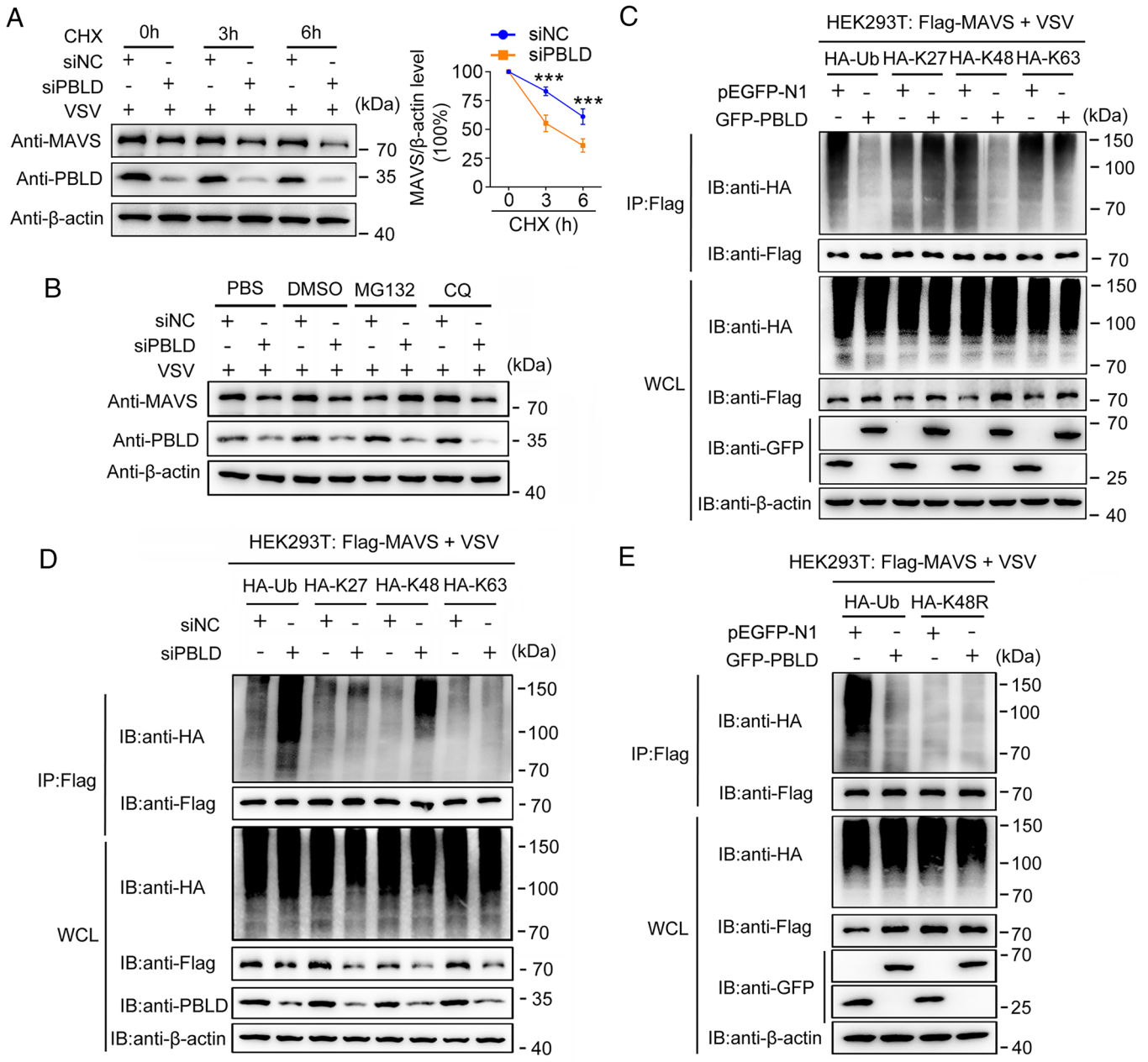

Fig. 4. PBLD inhibits MAVS degradation by mediating its K48-linked ubiquitination. (*A*) Western blotting analysis of the protein expression of MAVS in HeLa cells transfected with siPBLD or siNC and infected with VSV (MOI = 0.1) for 12 h, followed by treated with CHX for the indicated time points. Right, quantification of the expression levels of MAVS. (*B*) Western blotting analysis of the protein expression of MAVS in HeLa cells transfected with siPBLD or siNC and infected with VSV (MOI = 0.1) for 12 h, followed by treated with PBS, DMSO, MG132, and CQ. (*C*–*E*) IP and western blotting analysis of the ubiquitination of MAVS in HEK293T cells infected with VSV (MOI = 0.1) for 12 h; transfected with the plasmids GFP vector or GFP-PBLD together with Flag-MAVS, HA-Ub, HA-K27, HA-K48, or HA-K63 (*C*), respectively; transfected with the plasmids Flag-MAVS, HA-Ub, HA-K27, HA-K48, HA-K63, or siPBLD or siNC (*D*); or transfected with the plasmids Flag-MAVS, HA-Ub, HA-K48R, GFP-PBLD, or empty vector (*E*). Data in (*A*–*E*) are representative of one of three independent experiments. The quantification of the expression levels of MAVS after CHX treatment are presented as mean ± SD from three independent experiments, two-way ANOVA, ***$P < 0.001$.

Next, we investigated the involvement of PBLD in MAVS ubiquitination during virus infection. We found that MAVS ubiquitination was readily detected in the absence of PBLD overexpression, whereas cotransfection with Flag-PBLD significantly decreased MAVS ubiquitination (*SI Appendix*, Fig. S4 *G* and *H*). These findings suggest that PBLD stabilizes MAVS protein expression by mediating its deubiquitination. Previous studies have reported that various ubiquitin mutants, such as K27, K48, and K63, are associated with the ubiquitination of MAVS, particularly the K48 polyubiquitination chain, which is primarily involved in MAVS degradation (24, 25). In our investigation, we observed that PBLD reduced the number of K48-linked polyubiquitin chains associated with MAVS in VSV-infected HEK293T cells, but not in mock infection (Fig. 4*C* and *SI Appendix*, Fig. S4*I*). Conversely, the knockdown of PBLD prominently increased the levels of wild-type Ub and the ubiquitin mutant K48 but not the K27 or K63 mutants in VSV-infected HeLa cells (Fig. 4*D* and *SI Appendix*, Fig. S4*J*). Moreover, PBLD specifically blocked the ubiquitination of MAVS and had no effect on the K48-linked ubiquitination of other proteins (*SI Appendix*, Fig. S4*K*). Notably, PBLD had no significant impact on the ubiquitination of MAVS in combination with the ubiquitin mutant K48R (in which only Lys48 was mutated to Arg) (Fig. 4*E* and *SI Appendix*, Fig. S4*L*). Overall, these findings indicate that PBLD rescues MAVS from proteasome-dependent degradation by deconjugating K48-linked ubiquitin chains from MAVS during viral infection.

PBLD Deconjugates the K48-Linked Ubiquitin Chain from MAVS at Lys461 via USP4. To investigate the possible molecular mechanism underlying the inhibitory effect of PBLD on MAVS ubiquitination, we pulled down MAVS from virus-infected cells overexpressing MAVS, and the MAVS-bound proteins were subsequently analyzed via LC–MS/MS (*SI Appendix*, Fig. S5 *A* and *B*). Among these proteins, the deubiquitinating enzyme USP4 is a potential candidate for regulating MAVS expression since overexpression of PBLD reduced the K48-linked ubiquitination of MAVS during virus infection (*SI Appendix*, Fig. S5*C*). First, we verified the interaction between USP4 and MAVS during virus infection through the use of a coimmunoprecipitation assay (*SI Appendix*, Fig. S5 *D* and *E*). Subsequently, we found that overexpression of PBLD significantly augmented the interaction between USP4 and MAVS in the context of viral infection (Fig. 5*A*), but PBLD did not directly target USP4 (*SI Appendix*, Fig. S5*F*). This finding suggested that USP4 might be involved in the regulation of RNA virus-triggered signaling enhancement facilitated by PBLD. To identify the domain involved in the interaction between USP4 and MAVS, we created truncation mutants of USP4 and MAVS (Fig. 5 *B* and *C*). A coimmunoprecipitation assay demonstrated that USP4 coprecipitated with the MAVS mutant containing the CARD but did not coprecipitate with the mutant lacking the CARD (Fig. 5*B*). In addition, the interaction between MAVS and USP4 was found to depend on the N-terminal DUSP domain of USP4, whereas the C-terminal USP domain was not implicated (Fig. 5*C*). Moreover, overexpression of USP4 did not increase the expression of the shorter MAVS, which a N-terminally truncated isoform translationally initiated at M142 (*SI Appendix*, Fig. S5*G*). Next, we investigated the involvement of USP4 in the ubiquitination of MAVS during viral infection. Three siRNAs targeting USP4 (siUSP4) were successfully designed (*SI Appendix*, Fig. S5*H*). Our results revealed that depletion of USP4 resulted in augmented basal MAVS ubiquitination. Specifically, we observed an increase in the K48-linked polyubiquitination of MAVS, whereas K63-linked polyubiquitination did not significantly change (Fig. 5*D*). The lysine residues responsible for ubiquitination were identified via the UbPred program. We individually mutated five lysine (K) residues of MAVS to arginine (R) to generate the K7R, K311R, K362R, K461R, and K500R mutants. Coimmunoprecipitation assays demonstrated that only the K461R mutation increased the level of MAVS ubiquitination mediated by USP4 (Fig. 5*E*). To further clarify the site-specific role of USP4 in regulating MAVS function, we used MAVS-knockout cells (*SI Appendix*, Fig. S5*I*) and found that silencing USP4 expression leading to a decrease of *Ifnα4, Ifnb, and Isg15* expression in MAVS KO cells reconstituted with MAVS (WT) instead of MAVS (K461R) following virus infection (*SI Appendix*, Fig. S5*J*). Additionally, the deubiquitination of MAVS by USP4 was shown to be dependent on its DUB enzymatic activity because the catalytically inactive USP4 mutant, specifically USP4 (C311A), failed to deubiquitinate MAVS in VSV-infected cells (Fig. 5*F*). These results indicate that PBLD facilitates the deconjugation of K48-linked polyubiquitination of MAVS at K461 through the enzymatic activity of USP4.

PBLD Promotes the Expression of USP4 by Up-Regulating p53 to Enhance Antiviral Innate Immunity. We subsequently investigated how PBLD regulates the antiviral signaling pathway involving USP4. First, overexpression of PBLD led to increases in both the mRNA and protein levels of USP4 during virus infection (Fig. 6*A*), and silencing of PBLD had the opposite effect (Fig. 6*B*), suggesting that PBLD regulates USP4 transcription. Subsequently, we used the GeneCards and PROMO databases to identify seven potential binding sites for transcription factors within the sequence region from −1,000 to −1 of the USP4 promoter (Fig. 6*C*). Quantitative RT–PCR analysis revealed that PBLD overexpression up-regulated *p53* most obviously during virus infection, while silencing PBLD had the opposite effect (Fig. 6 *D* and *E*), speculating that the PBLD-mediated upregulation of USP4 mRNA expression is correlated with p53. Notably, the JASPAR CORE database was used to construct position weight matrices (PWMs) for p53 binding at specific sites within the USP4 promoter sequence (Fig. 6*F*). We further investigated the role of p53 in regulating USP4 expression and found that overexpression of p53 during virus infection led to increases in both the mRNA and protein levels of USP4 (Fig. 6*G*). Conversely, silencing p53 had the opposite effect (Fig. 6*H*). Subsequently, we constructed four luciferase reporters containing the USP4 promoter, which included mutants whose single binding sites and both binding sites were altered, and the luciferase reporter analysis demonstrated that p53 significantly increased the activity of the USP4 promoter when single binding sites were present but not when both binding sites were mutated (Fig. 6*I*). Chromatin immunoprecipitation (ChIP) assays revealed specific binding sites within the promoter region of USP4 in the regions spanning from −930 to −924 and from −72 to −66 (Fig. 6*J*). However, immunoprecipitation assays showed that there was no interaction between PBLD and p53 (*SI Appendix*, Fig. S6*A*). Our data further revealed that overexpression or knockout PBLD promoted or inhibited the expression of total p53 and phosphorylation of p53 at serine (Ser) 33 following virus infection (Fig. 6*K* and *SI Appendix*, Fig. S6*B*). Importantly, the phosphorylation of p53 at Ser33 is closely associated with its transcriptional activity in cellular processes (26–28). Furthermore, we revealed that PBLD increases p53 expression via activating the upstream signaling protein AP-1, but not p38, JNK, or other proteins, to promote p53-mediated transcriptional activation of USP4 (*SI Appendix*, Fig. S10 *A*–*C*). To further verify that PBLD participates in antiviral innate immunity by promoting the p53–USP4–MAVS signaling axis, we conducted a luciferase reporter assay. Consistent with our expectations, knocking down p53 or USP4 in HEK293T cells via siRNAs significantly attenuated the activation of the IFN-β promoter by PBLD compared with that in the control group upon VSV stimulation (Fig. 6*L*). Similarly, silencing p53 or USP4 disrupted the PBLD-induced upregulation of *Ifnb*, *Isg15*, and *Mx1* mRNA expression upon virus stimulation (Fig. 6*M* and *SI Appendix*, Fig.S6 *C* and *D*), and increased MAVS K48-linked ubiquitination, which reduced its protein expression (*SI Appendix*, Fig. S6 *E* and *F*). Since p53 and USP4 have roles in cell death induction, we also investigated the apoptosis involving PBLD/p53/USP4. Although PBLD induced cell apoptosis, especially at 24 h after VSV infection. However, overexpression of PBLD increased the total protein levels of p53 and p-p53 (S33), but not p-p53 (S46) (*SI Appendix*, Fig. S10*D*), which is associated with p53-induced apoptosis (29). We conjecture that the PBLD-mediated upregulation of p53 mainly plays a role in USP4 transcription during virus infection because the degree of cell apoptosis triggered by PBLD did no change after knockdown of p53 or USP4 (*SI Appendix*, Fig. S10*E*). These findings confirmed the mechanism by which PBLD enhances antiviral immunity and restrains RNA virus replication via the p53–USP4–MAVS signaling axis (Fig. 6*N*).

PBLD Deficiency Aggravates RNA Virus Infection in Mice. To further elucidate the functional significance of PBLD in host antiviral immunity, we analyzed age- and sex-matched $Pbld^{+/+}$ and $Pbld^{-/-}$ mice infected with VSV or H1N1, followed by various analyses (Fig. 7*A* and *SI Appendix*, Fig. S7*A*). Compared with those of wild-type littermates, the loss of body weight and clinical

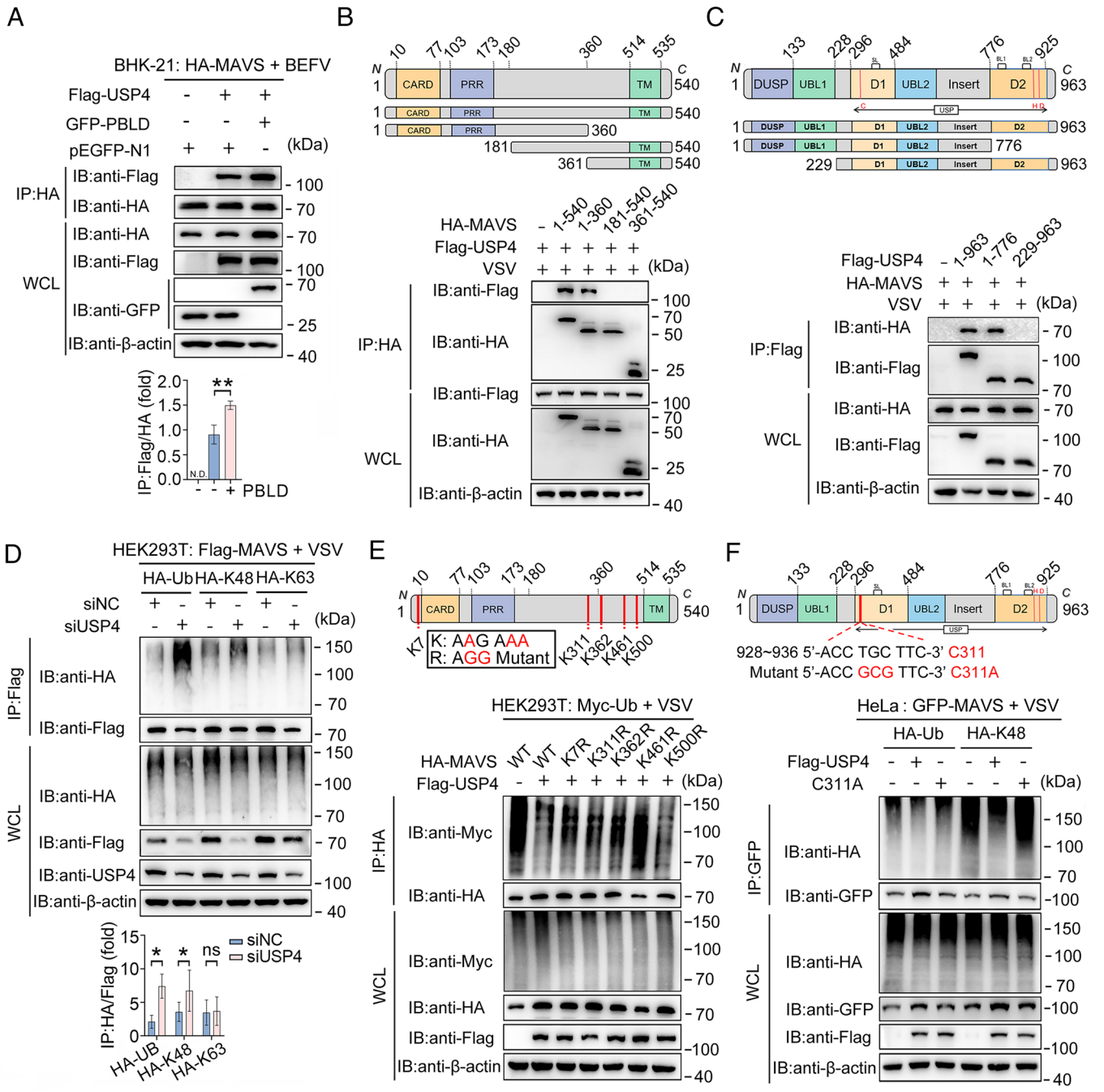

Fig. 5. PBLD promotes the binding and deubiquitination of MAVS by USP4. (*A*) IP and western blotting analysis of the indicated proteins in BHK-21 cells infected with BEFV (MOI = 0.1) for 12 h and transfected with the indicated plasmids of GFP-PBLD, HA-MAVS, and Flag-USP4, and quantitative analysis of the statistical data showing the expression levels of Flag/HA in Co-IP assay were analyzed using ImageJ software (*Bottom*). (*B* and *C*) Schematic diagram of MAVS (*B*) and USP4 (*C*) mutant constructs in *Above*. IP and western blotting analysis of the indicated proteins in HeLa cells infected with VSV (MOI = 0.1) for 12 h transfected with the indicated plasmids of Flag-USP4 and HA-MAVS mutants (*B*) or HA-MAVS and Flag-USP4 mutants (*C*) in *Bottom*. (*D–F*) IP and western blotting analyses of the ubiquitination of MAVS in HEK293T cells or HeLa cells infected with VSV (MOI = 0.1) for 12 h; transfected with the indicated plasmids for Flag-MAVS, HA-Ub, HA-K48, HA-K63, or the USP4-specific siRNA (siUSP4) or siNC (*D*), and quantitative analysis of the statistical data showing the expression levels of HA/Flag in Co-IP assay were analyzed using ImageJ software (*Bottom*); transfected with the indicated plasmids for Flag-USP4, Myc-Ub, HA-MAVS, and HA-MAVS mutants (*E*); or transfected with the plasmids for GFP-MAVS, HA-Ub, HA-K48, Flag-USP4, and Flag-USP4 mutants (*F*). Data in (*A–F*) are representative of one of three independent experiments. Data in (*A* and *D Bottom*) quantitative analysis of the statistical data are presented as mean ± SD from three independent experiments, Student's *t* test, ns $P > 0.05$, $^{*}P < 0.05$, and $^{**}P < 0.01$.

scores were greater in *Pbld*$^{-/-}$ mice infected with VSV (Fig. 7 *B* and *C*) or H1N1 (*SI Appendix*, Fig. S7 *B* and *C*), and there was a marked decrease in survival (Fig. 7*D* and *SI Appendix*, Fig. S7*D*), as well as significant alveolar wall thickening, immune cell infiltration, and tissue injury in the lungs or liver tissues upon VSV infection (Fig. 7*E* and *SI Appendix*, Fig. S7*E*) or H1N1 infection (*SI Appendix*, Fig. S7 *F* and *G*). In vivo, the protein of IFN-β was lower in the serum of *Pbld*$^{-/-}$ mice than in those of *pbld*$^{+/+}$ littermates following VSV or H1N1 infection (Fig. 7*F* and *SI Appendix*, Fig. S7*H*). Consistent with these findings, the viral loads of VSV and H1N1 were significantly greater in the organs of *Pbld*$^{-/-}$ mice than in those of control mice (Fig. 7*G* and *SI Appendix*, Fig. S7 *I* and *J*). Accordingly, the low mRNA levels of *Ifnb* and *Isg56* as well as MAVS protein expression and higher viral genes and proteins were observed in the organs of *Pbld*$^{-/-}$ mice than in those of *pbld*$^{+/+}$ littermates following VSV or

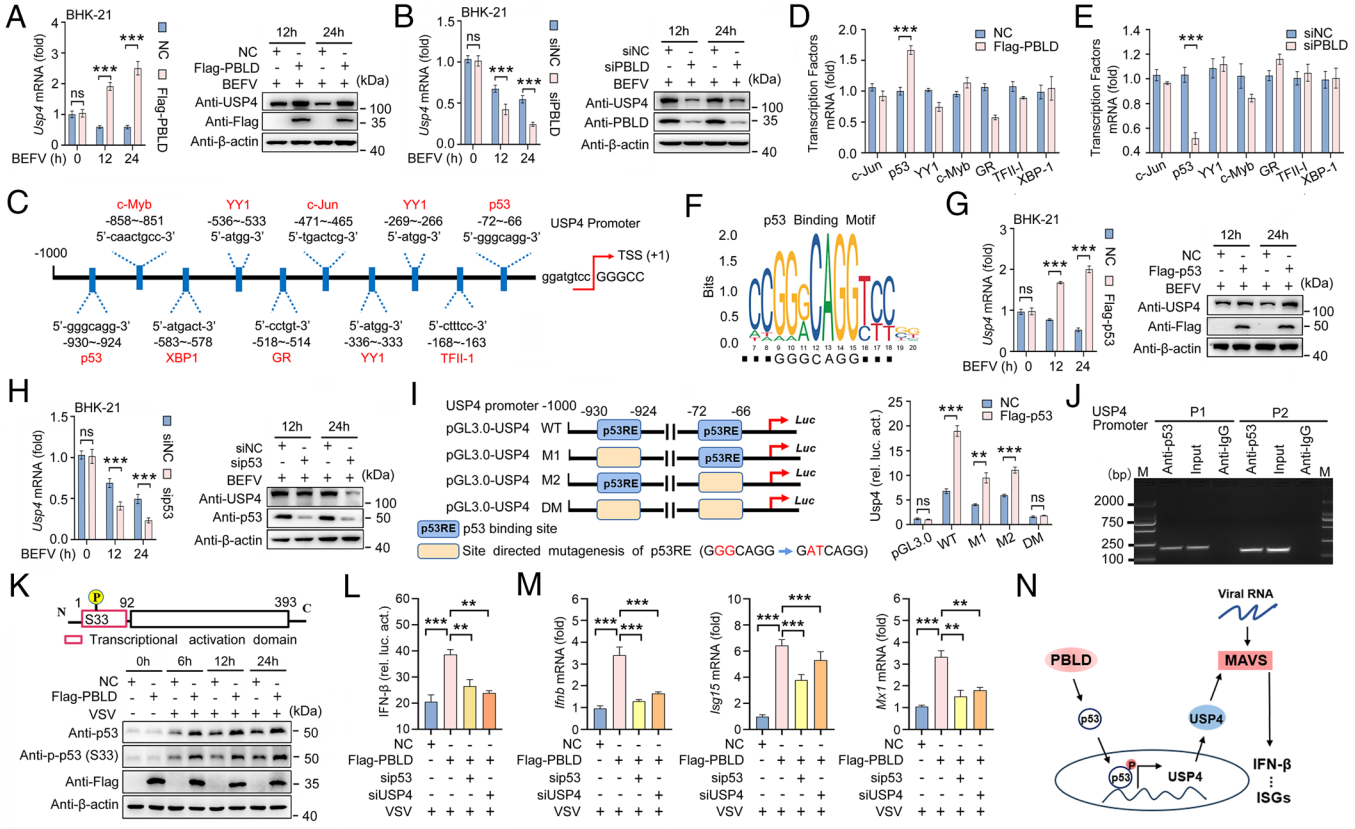

Fig. 6. The p53 orchestrates USP4 expression by binding its promoter region. (*A* and *B*) Real-time PCR analysis and western blotting analysis of the gene (*Left*) and protein (*Right*) levels of USP4 in BHK-21 cells infected with BEFV (MOI = 0.1) for the indicated time points and transfected with Flag-PBLD or control vector (*A*), and siPBLD or siNC (*B*). (*C*) Schematic diagram of the transcription factors that bind the USP4 promoter sequence. (*D* and *E*) Real-time PCR analysis of the expression of the indicated genes in HeLa cells transfected with Flag-PBLD or control vector (*D*) and siPBLD or siNC (*E*) with VSV infection (MOI = 0.1) for 12 h. (*F*) The potential binding sites of p53 in the promoter sites of USP4. (*G* and *H*) Real-time PCR analysis and western blotting analysis of the gene (*Left*) and protein (*Right*) expression levels of USP4 in BHK-21 cells infected with BEFV (MOI = 0.1) for the indicated time points and transfected with Flag-p53 (*G*) or p53-specific siRNA (sip53) or siNC (*H*), respectively. (*I*) Luciferase reporter assays were performed with HEK293T cells transfected with pRL-TK, USP4-Luc promoter plasmids, or USP4-Luc promoter mutants; together with Flag-p53 or empty vector; and infected with VSV (MOI = 0.1) for 12 h. (*J*) ChIP analysis of direct p53 binding to the USP4 promoter region in vivo. Rabbit IgG was used as a negative control. (*K*) Western blotting analysis of the protein expression of p53 and p-p53 (Ser33) in HeLa cells transfected with Flag-PBLD or empty vector and infected with VSV (MOI = 0.1) for the indicated times. (*L*) Luciferase reporter assays of HEK293T cells transfected with IFN-β-Luc promoter plasmids, pRL-TK, and the indicated siRNA with the Flag-PBLD plasmid or empty vector infected with VSV (MOI = 0.1) for 12 h. (*M*) Real-time PCR analysis of the mRNA levels of *Ifnb*, *Isg15*, and *Mx1* in HeLa cells transfected with the indicated siRNA and the Flag-PBLD plasmid or empty vector infected with VSV (MOI = 0.1) for 12 h. (*N*) A model by which PBLD enhances the type-I IFN response via the p53–USP4–MAVS signaling axis. Data in (*Right* of *A*, *B*, *G*, *H*, and *K*) are representative of one of three independent experiments. Data in (*Left* of *A*, *B*, *G*, *H* and *Right* of *I* and *D*, *E*, *L*, *M*) are presented as mean ± SD from three independent experiments, Student's *t* test or two-way ANOVA, ns $P > 0.05$, $^{**}P < 0.01$, and $^{***}P < 0.001$.

H1N1 infection (Fig. 7 *H* and *I* and *SI Appendix*, Fig. S7 *K–N*). These results demonstrated that PBLD deficiency significantly increases virulence and pathogenicity, exacerbating immune-mediated pathological development in mice.

Discussion

In this study, we demonstrated that PBLD can reduce the viral titers of BEFV, VSV, and H1N1. Furthermore, PBLD increased the increase in the mRNA expression of *Ifnb* and ISGs induced by viral infection or poly(I:C) transfection, indicating that PBLD plays an important role in the innate immune response to RNA viruses and in viral replication. Importantly, PBLD-deficient mice were more susceptible to VSV and H1N1 infection. This study reveals a unique biological function of PBLD as a positive regulator involved in the antiviral immune response and the regulation of RNA virus replication both in vitro and in vivo in a mouse model. However, the specific mechanism still needs to be further studied.

The RLR signaling pathway plays a crucial role in detecting RNA viruses (30, 31) and the host antiviral immune response (3, 32). The cGAS-STING pathway is responsible for recognizing cytoplasmic DNA and defending against DNA viruses (33–35). Here, we found that PBLD promotes innate immunity against RNA virus via the RIG-I/MAVS pathway. Furthermore, PBLD increased IFN/ISGs via RLRs, TLRs, and cGAS/STING respective stimuli. However, how the activity of PBLD extends to other PRRs, thereby promoting antiviral innate responses against viral infections, are worth further in-depth study. Several studies have suggested that MAVS plays critical roles in virus-triggered signaling. We observed a significant decrease in the protein level but not the mRNA level of MAVS in PBLD-knockdown and PBLD-knockout cells during RNA virus infection. These findings indicate that PBLD regulates the stability of the MAVS protein. Additionally, MG132 treatment confirmed that PBLD stabilizes MAVS protein expression through the ubiquitin–proteasome system.

Posttranslational modifications strictly control the activity and availability of MAVS. The process of ubiquitination is reversible and balanced by the activity of both E3 ligases and DUBs. While numerous E3 ligases have been shown to catalyze K48-linked ubiquitination and subsequent degradation of MAVS, the number of identified DUBs that modulate MAVS ubiquitination is limited. In our study, we conducted mass spectrometry analysis and identified USP4 as a specific DUB that targets MAVS. We found

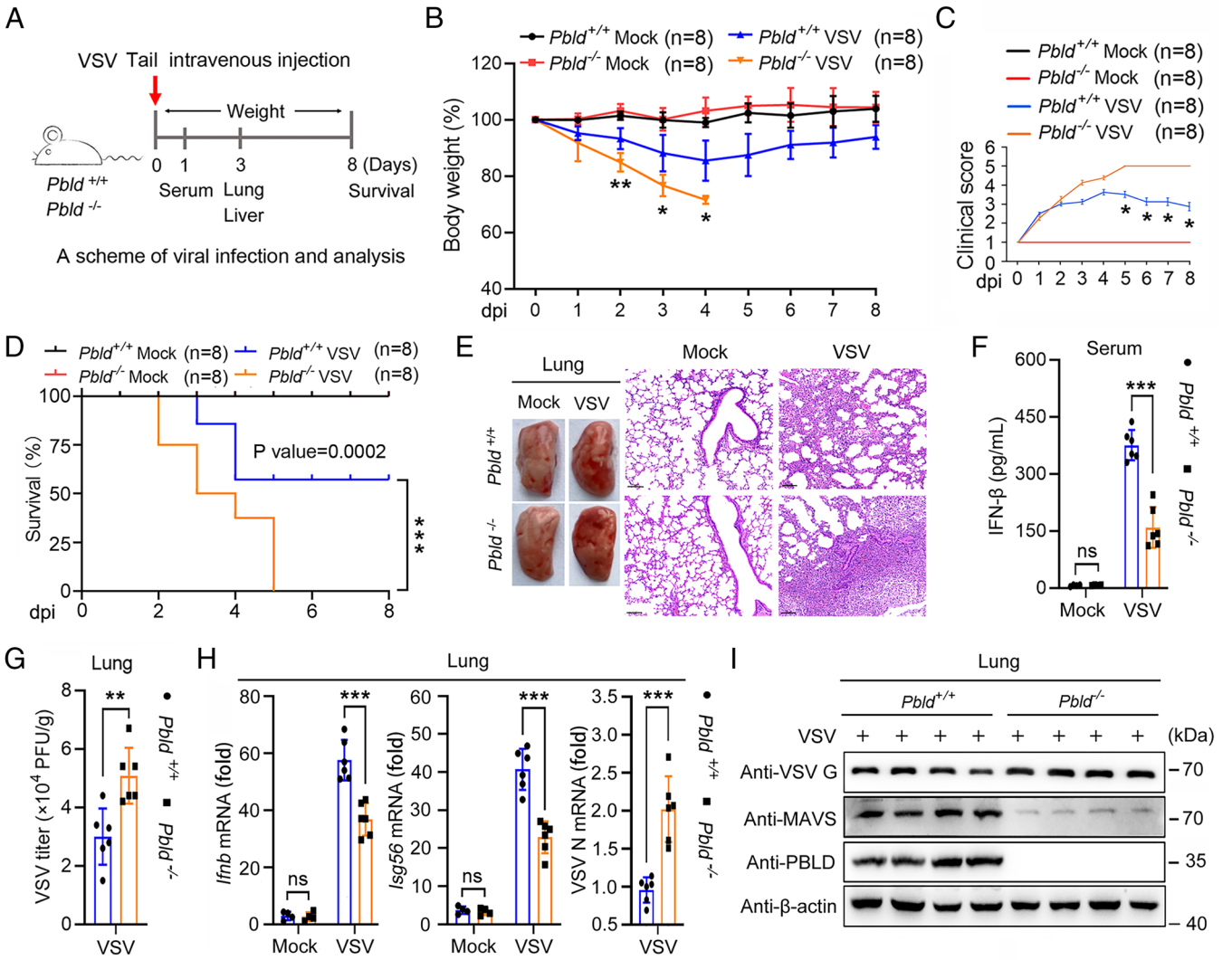

Fig. 7. PBLD-deficient mice are more susceptible to VSV infection. (*A*) Schematic of eight-week-old *Pbld*$^{+/+}$ and *Pbld*$^{-/-}$ mice were injected with VSV (1×10^8 PFU per mouse) via the tail vein, respectively. (*B* and *C*) Body weight following VSV infection in the first 8 d (n = 8) (*B*) and Clinical score (*C*). (*D*) Survival was estimated by the Kaplan–Meier method and compared by the two-sided log-rank test (n = 8). (*E*) Hematoxylin and eosin (H&E) staining of the lungs from *Pbld*$^{+/+}$ and *Pbld*$^{-/-}$ mice with VSV infection. (Scale bar, 100 μm.) (*F*) ELISA of IFN-β levels in the serum from *Pbld*$^{+/+}$ and *Pbld*$^{-/-}$ mice with VSV infection. (*G*) Viral titers were quantified by plaque assay of samples of the lungs from *Pbld*$^{+/+}$ and *Pbld*$^{-/-}$ mice with VSV infection. (*H* and *I*) Real-time qPCR and western blotting analysis of the mRNA levels of *Ifnb*, *Isg56,* and VSV *N* (*H*) and the indicated proteins in lung (*I*), respectively. Data in (*E* and *I*) are representative of one of three independent experiments. Data in (*B*, *C*, and *F–H*) are presented as mean ± SD from three independent experiments, Student's *t* test or two-way ANOVA, ns $P > 0.05$, *$P < 0.05$, **$P < 0.01$, and ***$P < 0.001$. Kaplan–Meier curves in *D*.

that USP4 participates in the PBLD-regulated antiviral immune response by deubiquitinating its target protein MAVS. For instance, USP4 functions as a positive regulator of type-I IFN signaling by removing K48-linked polyubiquitination chains from RIG-I or TRAF6 (36). Additionally, USP4 represses NF-κB activation by deubiquitinating K63-linked polyubiquitination chains from TRAF2, TRAF6, and TAK1 (37–39). In our research, we observed that USP4 knockdown enhances virus infection-induced K48-linked ubiquitination of MAVS and conjugation of Lys461 to MAVS, highlighting the crucial role of USP4 in positively regulating the innate antiviral immune response. In addition, we demonstrated that USP4 interacts with the N-terminal CARD of MAVS through residues 1 to 776 in this domain, demonstrating the importance of the USP4 N-terminal dually specific phosphatase (DUSP) domain in maintaining the stability of MAVS protein expression. These findings align with the binding requirements between USP4 and Rheb or ARF-BP1 (40). Another study reported that under physiological conditions, USP4 interacts with the N-terminal CARD of RIG-I (36). A recent study revealed that USP4-WT, but not the USP4-C311A mutant, inhibits TNF-α-induced TAK1 polyubiquitination (37). Similarly, USP4 promotes TNF-α-induced apoptosis through the deubiquitination of RIP1, whereas the USP4-C311S mutant does not (41). These results demonstrated the essential role of enzymatic activity in maintaining the deubiquitination function of USP4. Consistent with these findings, we found that USP4, but not the USP4-C311A mutant, decreased the VSV-induced ubiquitination of MAVS, suggesting that the deubiquitination of MAVS by USP4 relies on its enzymatic activity. Notably, overexpression of USP4 did not increase the expression of the shorter MAVS, suggesting that this regulation may be dependent on the interaction of USP4 with the MAVS N-terminal region. In brief, this study reports that USP4 regulates MAVS to promote the innate antiviral immune response.

Although the biological function of USP4 has been investigated in multiple aspects, there is still limited knowledge about its transcriptional regulatory mechanism involving specific transcription factors. A report has shown that the transcriptional repressor 1 of the snail family (Snail1) up-regulates USP4 transcriptionally by

binding to its promoter region (42). Through ChIP analysis and luciferase reporter assays, our investigation revealed that p53 positively regulates the expression of USP4 by directly binding to the −930 to −924 site and the −72 to −66 site of the USP4 gene. P53, encoded by the *TP53* gene, is a transcription factor that is activated in response to various stresses and controls a variety of biological processes, such as cell apoptosis and viral replication through the regulation of its target genes. Previous studies have shown that p53 can be activated by viral infection, limiting viral replication and promoting host antiviral defense mechanisms (43). Moreover, there are negative correlations between the overexpression of p53 and the replication of various viruses, such as IAV (44) and porcine epidemic diarrhea virus (PEDV) (45). However, our results show that PBLD promotes cell apoptosis induced by viral infection, but not associated with p53 and USP4, although, which are well-known roles in cell death. These findings further emphasize the critical role of the PBLD-mediated regulation of p53 in the innate antiviral immune response.

In conclusion, we identified PBLD as a key molecule that is involved in the host antiviral immune response to RNA virus infection. Our findings lead to the proposal of a combinational model in which PBLD promotes the innate immune response via the p53–USP4–MAVS signaling axis (*SI Appendix*, Fig. S10). Consequently, the regulation of the antiviral immune response by PBLD plays a critical role in determining virus replication and may be important for the development of drugs to combat RNA virus-mediated pandemics.

Materials and Methods

Cells, Viruses, and Mice. The cells and viruses that were used in our study are listed in the key resources table. A murine strain deficient in *Pbld2* and *Pbld1* was established with the help of Guangzhou Cyagen Biosciences, Inc. (20). The genotype of the $pbld^{-/-}$ mice was confirmed by PCR with the specific primers shown in *SI Appendix*, Table S2. All the animal experiments were performed in strict accordance with the State Council-approved People's Republic of China Regulations on the Administration of Experimental Animal Affairs (1 November 1988). The mice were handled according to the Shandong Normal University Institutional Animal Care and Use Committee (IACUC) policies on animal use.

Plasmid Construction and Generation of Stable Cell Lines. The specified PCR products were amplified with the primer pairs and subsequently cloned and inserted into different vectors, as shown in *SI Appendix*, Table S3. PBLD-overexpressing cell lines, PBLD- and MAVS- knockout (KO) cell lines were generated according to protocols described in previous studies (46). All the specific sequences of the primers that were used are shown in *SI Appendix*, Table S2.

Preparation of Mouse Primary Cells. PMs and BMDMs were isolated from $Pbld^{+/+}$ and $Pbld^{-/-}$ mice (8 to 10 wk old) as described previously (47). Briefly, PMs were collected from the peritoneal lavage after intraperitoneally injected with 3 mL of 4% sodium thioglycolate (Sigma, 70157) solution for 3 d. BMDMs were prepared from the femurs and tibias of the mice. Then, the cells were cultured in RPMI-1640 medium supplemented with 20 ng/mL murine M-CSF after 6 d for subsequent experiments.

Virus Preparation, Cell Infection, and Virus Titration. The BEFV and VSV used in this study were passaged in BHK-21 cells and HeLa cells, respectively. H1N1 plants were grown in 10-d-old fertilized eggs and stored at -80 °C. For H1N1 infection, MDCK cells were incubated with the virus diluted in Op-ti MEM supplemented with 1% penicillin/streptomycin and 0.5% μg/mL TPCK-treated trypsin (Sigma, T1426) for the indicated times. The H1N1 viral titer was measured via hemagglutination. The titer was expressed as $lgTCID_{50}$/mL, as determined by the Reed–Muench endpoint method. Virus plaque assays were performed by serially diluting VSV or H1H1 and then using these dilutions to infect Vero cells. After the cells were incubated with DMEM containing 2% methylcellulose for 48 h, the cells were fixed with 4% paraformaldehyde and stained with 1% crystal violet. Finally, the plaques were counted, averaged, and multiplied by the dilution factor to determine the viral titer as PFU/ml.

Luciferase Reporter Assays. HEK293T cells were transiently transfected with the firefly luciferase reporter and the TK-Renilla luciferase internal control plasmid with or without the indicated plasmids. The cells were lysed and analyzed with a dual-luciferase reporter assay kit according to the manufacturer's instructions.

Protein Half-Life Assays. Cells with silencing of PBLD in 6-well plates were infected with VSV or BEFV, before being treated with the protein synthesis inhibitor cycloheximide (CHX, 100 μg/mL) for the indicated times. Cells were then collected and analyzed by immunoblotting with the indicated antibodies.

Quantitative Real-Time PCR and ELISA. Total RNA was extracted via a cell total RNA kit (Foregene, RE-03111) and the cDNA was reverse transcribed with cDNA synthesis supermix (Accurate, AG11706) according to the manufacturer's protocol, RT−qPCR analysis was performed with SYBR Green PCR Master Mix. β-actin or GAPDH were used as an internal control. All primers are listed in *SI Appendix*, Table S2. Mouse ELISA kits for IFN-β and IFN-α in serum or cell culture supernatants were measured according to the manufacturer's instructions.

Western Blotting Analysis and Immunoprecipitation (IP). Western blotting analysis was performed as described previously (31). For immunoprecipitation, whole-cell extracts were lysed by lysis buffer supplemented with protease inhibitor. Subsequently, the supernatants were incubated with protein A/G magnetic beads and the corresponding antibodies. The immunoprecipitates were eluted and separated by SDS–PAGE (Epizyme Biotech, PG113) and transferred to polyvinylidene fluoride membranes (Millipore, IPVH00010). After blocked with 5% nonfat dry milk (BioFroxx, 1172), the membranes were incubated with the indicated antibodies.

Chromatin Immunoprecipitation (ChIP) Assay. Briefly, HeLa cells were cross-linked with 1% formaldehyde and stopped with 0.1 mol/L glycine. Then, the cell lysates were sonicated and subjected to immunoprecipitation using an anti-p53 antibody and normal IgG. After reversal of cross-links, precipitated DNA fragments were recovered and amplified by PCR with primers listed in *SI Appendix*, Table S2.

Gross Examination and Histological Analysis. Body weight and clinical scoring were performed during VSV and H1N1 infection, and the results were scored according to previous methods (48) as follows: healthy mouse = 1; mouse showing signs of malaise = 2; mouse showing signs of strong piloerection, constricted abdomen, changed gait, and periods of inactivity = 3; mouse with enhanced characteristics of the previous group but showing little activity and becoming moribund = 4; and dead mouse = 5. The lung histological scores were measured following a standardized scoring system as previously described (49). The mean value of three random areas in each lung tissue sample was calculated. The scores were as follows: 0, no damage; 1, mild damage; 2, moderate damage; 3, marked damage; and 4, severe histological changes.

Protein Ubiquitination Analysis. HEK293T cells were transfected with the indicated plasmids and treated with VSV or mock infection. The cells were then lysed, and the supernatants were incubated with Protein G Sepharose beads coupled to specific antibodies. The bound proteins were eluted and subjected to immunoblotting analysis with the indicated antibodies.

Mass Spectrometry. BHK21 cells were transfected with HA-MAVS and Flag-PBLD or vector control plasmid and infected with BEFV for 24 h. Cell lysate was immunoprecipitated with anti-HA antibody–conjugated agarose beads overnight. A 10% PAGE gel was used for Immunoprecipitated protein and Coomassie gel staining analysis. Then, the gel was sent for mass spectrometry.

Quantification and Statistical Analysis. Statistical analysis was performed via GraphPad Prism 8.0.2 software. Comparisons between the different groups were performed by Student's *t* test or two-way ANOVA was used for multiple comparisons between grouped graphs or multiple samples. The results are presented as the mean values ± SD from at least three independent experiments. The western blotting band intensities were analyzed via ImageJ software. Survival of $Pbld^{+/+}$ and $pbld^{-/-}$ mice was examined via Kaplan–Meier survival analysis. Values for which $^{*}P < 0.05$, $^{**}P < 0.01$, and $^{***}P < 0.001$ were considered statistically significantly different, and ns indicates a nonsignificant difference $P > 0.05$.

Data, Materials, and Software Availability. All study data are included in the article and/or supporting information, research datasets (50).

ACKNOWLEDGMENTS. This study was partially supported by Grants from the National Natural Science Fund of China (32373000 and 32072834) and Shandong Provincial Natural Science Foundation, China (ZR2021MC050). We are thankful to the organization American Journal Experts for the English language reviewing.

Author affiliations: [a]Ruminant Diseases Research Center, Key Laboratory of Animal Resistant Biology of Shandong, College of Life Sciences, Shandong Normal University, Jinan 250358, People's Republic of China; [b]Department of Preventive Veterinary Medicine, College of Veterinary Medicine, Shandong Agricultural University, Taian 271018, People's Republic of China; [c]State Key Laboratory of Zoonosis Research, Ministry of Education, College of Veterinary Medicine, Jilin University, Changchun 130062, People's Republic of China; [d]The College of Arts and Sciences, University of North Carolina at Chapel Hill, Chapel Hill, NC 27599; and [e]Changchun Veterinary Research Institute, Chinese Academy of Agricultural Sciences, Changchun 130122, People's Republic of China

1. L. Jiang, H. Chen, C. Li, Advances in deciphering the interactions between viral proteins of influenza A virus and host cellular proteins. *Cell Insight* **2**, 100079 (2023).
2. A. Nemudryi *et al.*, SARS-CoV-2 genomic surveillance identifies naturally occurring truncation of ORF7a that limits immune suppression. *Cell Rep.* **35**, 109197 (2021).
3. K. Onomoto, K. Onoguchi, M. Yoneyama, Regulation of RIG-I-like receptor-mediated signaling: Interaction between host and viral factors. *Cell Mol. Immunol.* **18**, 539–555 (2021).
4. H. Zhu, C. Zheng, When PARPs meet antiviral innate immunity. *Trends Microbiol.* **29**, 776–778 (2021).
5. Y. M. Loo *et al.*, Distinct RIG-I and MDA5 signaling by RNA viruses in innate immunity. *J. Virol.* **82**, 335–345 (2008).
6. H. Kato *et al.*, Differential roles of MDA5 and RIG-I helicases in the recognition of RNA viruses. *Nature* **441**, 101–105 (2006).
7. F. Hou *et al.*, MAVS forms functional prion-like aggregates to activate and propagate antiviral innate immune response. *Cell* **146**, 448–461 (2011).
8. W. Zeng *et al.*, Reconstitution of the RIG–I pathway reveals a signaling role of unanchored polyubiquitin chains in innate immunity. *Cell* **141**, 315–330 (2010).
9. R. B. Seth, L. Sun, C. K. Ea, Z. J. Chen, Identification and characterization of MAVS, a mitochondrial antiviral signaling protein that activates NF-kappaB and IRF 3. *Cell* **122**, 669–682 (2005).
10. E. Meylan *et al.*, Cardif is an adaptor protein in the RIG-I antiviral pathway and is targeted by hepatitis C virus. *Nature* **437**, 1167–1172 (2005).
11. X. Chen *et al.*, Zebrafish sirt5 negatively regulates antiviral innate immunity by attenuating phosphorylation and ubiquitination of mavs. *J. Immunol.* **209**, 1165–1172 (2022).
12. S. Z. Li *et al.*, Phosphorylation of MAVS/VISA by Nemo-like kinase (NLK) for degradation regulates the antiviral innate immune response. *Nat. Commun.* **10**, 3233 (2019).
13. Y. L. Deribe, T. Pawson, I. Dikic, Post-translational modifications in signal integration. *Nat. Struct. Mol. Biol.* **17**, 666–672 (2010).
14. S. Wang *et al.*, DDIT3 targets innate immunity via the DDIT3-OTUD1-MAVS pathway to promote bovine viral diarrhea virus replication. *J. Virol.* **95**, e02351-20 (2021).
15. T. Liuyu *et al.*, Induction of OTUD4 by viral infection promotes antiviral responses through deubiquitinating and stabilizing MAVS. *Cell Res.* **29**, 67–79 (2019).
16. Y. Liang *et al.*, circKDM4C suppresses tumor progression and attenuates doxorubicin resistance by regulating miR-548p/PBLD axis in breast cancer. *Oncogene* **38**, 6850–6866 (2019).
17. D. M. Li *et al.*, MAWBP and MAWD inhibit proliferation and invasion in gastric cancer. *World J. Gastroenterol.* **19**, 2781–2792 (2013).
18. L. Han *et al.*, PBLD inhibits angiogenesis via impeding VEGF/VEGFR2-mediated microenvironmental cross-talk between HCC cells and endothelial cells. *Oncogene* **41**, 1851–1865 (2022).
19. A. Li *et al.*, Decreased expression of PBLD correlates with poor prognosis and functions as a tumor suppressor in human hepatocellular carcinoma. *Oncotarget* **7**, 524–537 (2016).
20. S. Chen *et al.*, Epithelial PBLD attenuates intestinal inflammatory response and improves intestinal barrier function by inhibiting NF-kappaB signaling. *Cell Death Dis.* **12**, 563 (2021).
21. Z. Qu *et al.*, A novel intronic circular RNA Antagonizes influenza virus by absorbing a microRNA that degrades CREBBP and accelerating IFN-beta production. *mBio* **12**, e0101721 (2021).
22. T. He *et al.*, Duck plague virus UL41 protein inhibits RIG-I/MDA5-mediated duck IFN-beta production via mRNA degradation activity. *Vet. Res.* **53**, 22 (2022).
23. R. T. Lin, Y. Mamane, J. Hiscott, Structural and functional analysis of interferon regulatory factor 3: Localization of the transactivation and autoinhibitory domains. *Mol. Cell. Biol.* **19**, 2465–2474 (1999).
24. Y. Y. Chen, X. H. Ran, R. Z. Ni, D. Mu, TRIM28 negatively regulates the RLR signaling pathway by targeting MAVS for degradation via K48-linked polyubiquitination. *J. Biol. Chem.* **299**, 104660 (2023).
25. K. Guan *et al.*, MAVS regulates apoptotic cell death by decreasing K48-linked ubiquitination of voltage-dependent anion channel 1. *Mol. Cell Biol.* **33**, 3137–3149 (2013).
26. L. M. M. Jenkins, S. R. Durell, S. J. Mazur, E. Appella, p53 N-terminal phosphorylation: A defining layer of complex regulation. *Carcinogenesis* **33**, 1441–1449 (2012).
27. H. Ruan *et al.*, Computational strategy for intrinsically disordered protein ligand design leads to the discovery of p53 transactivation domain I binding compounds that activate the p53 pathway. *Chem. Sci.* **12**, 3004–3016 (2021).
28. N. Raj, L. D. Attardi, The transactivation domains of the p53 protein. *Cold Spring Harb Perspect. Med.* **7**, a026047 (2017).
29. K. Yoshida, H. S. Liu, Y. Miki, Protein kinase C δ regulates Ser phosphorylation of p53 tumor suppressor in the apoptotic response to DNA damage. *J. Biol. Chem.* **281**, 5734–5740 (2006).
30. I. G. Nerbovik *et al.*, Molecular cloning of MDA5, phylogenetic analysis of RIG-I-like receptors (RLRs) and differential gene expression of RLRs, interferons and proinflammatory cytokines after in vitro challenge with IPNV, ISAV and SAV in the salmonid cell line TO. *J. Fish. Dis.* **40**, 1529–1544 (2017).
31. K. Wicherska-Pawlowska, T. Wrobel, J. Rybka, Toll-like receptors (TLRs), NOD-like receptors (NLRs), and RIG-I-like receptors (RLRs) in innate immunity. TLRs, NLRs, and RLRs ligands as immunotherapeutic agents for hematopoietic diseases. *Int. J. Mol. Sci.* **22**, 13397 (2021).
32. X. Li *et al.*, SARS-CoV-2 ORF10 suppresses the antiviral innate immune response by degrading MAVS through mitophagy. *Cell Mol. Immunol.* **19**, 67–78 (2022).
33. X. Cai, Y. H. Chiu, Z. J. J. Chen, The cGAS-cGAMP-STING pathway of cytosolic DNA sensing and signaling. *Mol. Cell* **54**, 289–296 (2014).
34. M. Zhang *et al.*, USP18 recruits USP20 to promote innate antiviral response through deubiquitinating STING/MITA. *Cell Res.* **26**, 1302–1319 (2016).
35. S. P. T. Yiu *et al.*, An Epstein-Barr virus protein interaction map reveals NLRP3 inflammasome evasion via MAVS UFMylation. *Mol. Cell* **83**, 2367 (2023).
36. L. Wang *et al.*, USP4 positively regulates RIG-I-mediated antiviral response through deubiquitination and stabilization of RIG-I. *J. Virol.* **87**, 4507–4515 (2013).
37. Y. H. Fan *et al.*, USP4 targets TAK1 to downregulate TNFalpha-induced NF-kappaB activation. *Cell Death Differ.* **18**, 1547–1560 (2011).
38. N. Xiao *et al.*, Ubiquitin-specific protease 4 (USP4) targets TRAF2 and TRAF6 for deubiquitination and inhibits TNFalpha-induced cancer cell migration. *Biochem. J.* **441**, 979–986 (2012).
39. F. Zhou *et al.*, Ubiquitin-specific protease 4 mitigates Toll-like/interleukin-1 receptor signaling and regulates innate immune activation. *J. Biol. Chem.* **287**, 11002–11010 (2012).
40. L. Deng *et al.*, Ubiquitination of Rheb governs growth factor-induced mTORC1 activation. *Cell Res.* **29**, 136–150 (2019).
41. X. Hou, L. Wang, L. Zhang, X. Pan, W. Zhao, Ubiquitin-specific protease 4 promotes TNF-alpha-induced apoptosis by deubiquitination of RIP1 in head and neck squamous cell carcinoma. *FEBS Lett.* **587**, 311–316 (2013).
42. R. Li *et al.*, LOXL3-promoted hepatocellular carcinoma progression via promotion of Snail1/USP4-mediated epithelial-mesenchymal transition. *Environ. Toxicol.* **37**, 2540–2551 (2022).
43. C. Rivas, S. A. Aaronson, C. Munoz-Fontela, Dual role of p53 in innate antiviral immunity. *Viruses* **2**, 298–313 (2010).
44. E. Turpin *et al.*, Influenza virus infection increases p53 activity: Role of p53 in cell death and viral replication. *J. Virol.* **79**, 8802–8811 (2005).
45. Z. Hao *et al.*, Tumor suppressor p53 inhibits porcine epidemic diarrhea virus infection via interferon-mediated antiviral immunity. *Mol. Immunol.* **108**, 68–74 (2019).
46. W. Ma, H. Wang, H. He, Bovine herpesvirus 1 tegument protein UL41 suppresses antiviral innate immune response via directly targeting STAT1. *Vet. Microbiol.* **239**, 108494 (2019).
47. H. S. Chang *et al.*, CD97 negatively regulates the innate immune response against RNA viruses by promoting RNF125-mediated RIG-I degradation. *Cell. Mol. Immunol.* **20**, 1457–1471 (2023).
48. G. A. Rossi, W. Bessler, S. Ballarini, C. Pasquali, Evidence that a primary anti-viral stimulation of the immune response by OM-85 reduces susceptibility to a secondary respiratory bacterial infection in mice. *Ital. J. Pediatr.* **44**, 112 (2018).
49. H. Yang *et al.*, The influenza virus PB2 protein evades antiviral innate immunity by inhibiting JAK1/STAT signalling. *Nat. Commun.* **13**, 6288 (2022).
50. F. Y. Chu, Data from "PBLD enhances antiviral innate immunity by promoting the p53-USP4-MAVS signaling axis." Figshare. http://doi.org/10.6084/m9.figshare.27637155.v1. Deposited 8 November 2024.